

PHYSICS

Field theory spin and momentum in water waves

Konstantin Y. Bliokh^{1*}, Horst Punzmann², Hua Xia², Franco Nori^{1,3}, Michael Shats^{2*}

Spin is a fundamental yet nontrivial intrinsic angular momentum property of quantum particles or fields, which appears within relativistic field theory. The spin density in wave fields is described by the theoretical Belinfante-Rosenfeld construction based on the difference between the canonical and kinetic momentum densities. These quantities are usually considered as abstract and non-observable per se. Here, we demonstrate, both theoretically and experimentally, that the Belinfante-Rosenfeld construction naturally arises in gravity (water surface) waves. There, the canonical momentum is associated with the generalized Stokes drift phenomenon, while the spin is generated by subwavelength circular motion of water particles. Thus, we directly observe these fundamental field theory properties as microscopic mechanical properties of a classical wave system. Our findings shed light onto the nature of spin and momentum in wave fields, demonstrate the universality of relativistic field theory concepts, and offer a new platform for their studies.

INTRODUCTION

Spin angular momentum was first introduced to physics empirically in 1925 by Uhlenbeck and Goudsmit (1, 2). This allowed them to explain peculiarities of the emission spectra of solids and electron interactions with magnetic fields by a quantum “self-rotation” of electrons. Later, this new property was derived rigorously within the Dirac equation that provides the quantum relativistic theory of electrons (3) and using relativistic field theory approaches (4–7). Nowadays, spin is essential for numerous quantum and condensed matter systems (2), ranging from basic properties of elementary particles and chemical elements, via widely used memory and tomography devices, to the advanced fields of spintronics (8, 9) and quantum computing (10–12).

As early as in 1909, Poynting (13) described the intrinsic angular momentum of circularly polarized light (i.e., an electromagnetic wave with rotating electric and magnetic field vectors). This property was later observed via optical torque on matter (14), and it was associated with the spin of photons (i.e., relativistic massless quanta of light) (3, 15–17). Thus, the spin angular momentum naturally appears in classical electromagnetic fields (16–19) where it plays an important role in optical manipulation, light-matter interactions, information transfer, etc. (16, 17, 20–22). In 1973, Jones (23) argued that intrinsic angular momentum, or spin, could be ascribed to classical nonrelativistic waves, such as acoustic and internal gravity waves in fluids. There, spin is associated with the mechanical angular momentum of the medium particles oscillating or moving along microscopic elliptical orbits in wave fields. This interpretation was essentially neglected [(23) was cited only eight times for almost half-century], and, recently, it was shown again that inhomogeneous acoustic (sound wave) fields have a nonzero spin angular momentum density (24–28). This time, the presence of acoustic spin was supported by the analogy between acoustic and electromagnetic waves and was confirmed experimentally (25).

Theoretically, various kinds of quantum and classical waves can be described within the corresponding field theories (3, 6). There,

one of the main objects characterizing dynamical properties of the field is the energy-momentum tensor, which includes the field energy and momentum densities and provides for the local energy-momentum conservation laws. In 1940, Belinfante and Rosenfeld (4–6) found a fundamental structure in this tensor, which explains the appearance of spin angular momentum and relates it to the momentum properties of the field. They showed that there are canonical (nonsymmetric, derived from the Noether theorem) and kinetic (symmetrized) versions of the energy-momentum tensor, which contain the corresponding canonical and kinetic momentum densities, \mathbf{P} and $\mathbf{\Pi}$, related as

$$\mathbf{\Pi} = \mathbf{P} + \frac{1}{2} \nabla \times \mathbf{S} \quad (1)$$

where \mathbf{S} is the spin angular momentum density. This fundamental relation describes the appearance of spin in both quantum particles and classical (electromagnetic and acoustic) wave fields (6, 7, 17, 19, 21, 23, 25, 28–30). According to Noether’s theorem, the integral values of both kinetic and canonical momentum densities are conserved in translation-invariant systems. In turn, rotational invariance is associated with the conservation of the integral angular momentum. Its density is given by $\mathbf{r} \times \mathbf{\Pi}$ in the kinetic picture and $\mathbf{r} \times \mathbf{P} + \mathbf{S}$ in the canonical one (6, 19, 28), where \mathbf{r} is the position vector.

Despite such progress and thorough exploration of spin in various fields, this fundamental physical entity remains nontrivial and is described by rather abstract quantum mechanical and relativistic field theory concepts (1–7). Indeed, the “self-rotation” of the electron described by the Dirac spinors is far from an intuitively clear picture. Furthermore, the canonical momentum and spin densities in the field theory relation Eq. 1 are usually regarded as unobservable per se (4–6), and only their integral values matter. In classical fields, rotating angular momentum properties underlying spin are more obvious, but rotating electric and magnetic fields in circularly polarized light (13–22) or rotating medium particles in inhomogeneous sound waves (23–28) are never observed directly.

The purpose of this work is multifold. First, we will describe and observe the presence of spin in another kind of wave field, namely, in gravity water surface waves (31). We will show that the water wave spin is described precisely by the same field theory relation Eq. 1 involving the canonical and kinetic momenta. This is unexpected, because water surface waves cannot be described by a relativistic

Copyright © 2022 The Authors, some rights reserved; exclusive licensee American Association for the Advancement of Science. No claim to original U.S. Government Works. Distributed under a Creative Commons Attribution NonCommercial License 4.0 (CC BY-NC).

¹Theoretical Quantum Physics Laboratory, RIKEN Cluster for Pioneering Research, Wako-shi, Saitama 351-0198, Japan. ²Research School of Physics, The Australian National University, Canberra, ACT 2601, Australia. ³Physics Department, University of Michigan, Ann Arbor, MI 48109-1040, USA.

*Corresponding author. Email: k.bliokh@gmail.com (K.Y.B.); michaelshat@gmail.com (M.S.)

Lagrangian field theory like electromagnetic or sound waves. This can be seen from the fact that electromagnetic and acoustic field theories are based on the properties of the Minkowski space-time and essentially involve linear dispersion $\omega = ck$ (ω is the frequency, k is the wave number, and c is the speed of light or sound), while water waves are inherently dispersive, e.g., $\omega = \sqrt{gk}$ in the deep-water approximation (g is the gravitational acceleration). Although there is a number of rather sophisticated Lagrangian and Hamiltonian approaches to fluid dynamics and water waves (32–35), they do not provide a simple unified picture of momentum and angular momentum of surface gravity waves, and, in contrast to their electromagnetic and acoustic counterparts, these fundamental quantities are almost never mentioned in textbooks on fluid dynamics (see the Supplementary Materials) and do not typically appear in experimental observations. Here, we argue that the concepts of spin and kinetic/canonical momenta, originating from relativistic field theory, illuminate and accurately describe the observable dynamical properties of surface gravity waves.

Second, we will provide the direct observation of the motion of water particles underlying the spin and canonical momentum densities in Eq. 1. In doing so, the local rotational motion of particles corresponds to the spin density \mathbf{S} , whereas the translational motion due to the generalized Stokes drift (36–38) corresponds to the canonical momentum density \mathbf{P} . To the best of our knowledge, this is the first direct observation of the microscopic origin of the spin angular momentum and canonical momentum in wave fields. Furthermore, the generalized Stokes drift described and observed in our work accurately characterizes the mass transport in acoustic and water wave fields and provides the directly observable momentum of these waves. This is crucial for numerous applications involving transport of microscopic and macroscopic objects in water waves.

Last, by comparing our approach to water waves with other wave theories, we demonstrate the universality of the spin, momentum, and Belinfante-Rosenfeld concepts across quantum systems, electromagnetism, acoustics, and hydrodynamics (although relativistic field theory is not directly applicable to water waves). This opens up new opportunities for both quantum relativistic and classical physics.

RESULTS

Basic spin and momentum properties of vector wave fields

To begin with, Table 1 lists the main dynamical quantities involved in Eq. 1, as well as the energy density, for monochromatic electromagnetic waves in free space (17–19, 21, 28–30) and sound waves in a fluid or gas (25–28). For all kinds of monochromatic waves with frequency ω , we consider complex space-dependent field amplitudes $\mathbf{F}(\mathbf{r})$, so that real time-dependent fields are $\mathbf{F}(\mathbf{r}, t) = \text{Re}[\mathbf{F}(\mathbf{r})e^{-i\omega t}]$. In this manner, electromagnetic waves are described by the complex vector electric and magnetic fields, $\mathbf{E}(\mathbf{r})$ and $\mathbf{H}(\mathbf{r})$, while acoustic waves are described by the complex vector velocity field $\mathbf{v}(\mathbf{r})$ and scalar pressure field $p(\mathbf{r})$. In both electromagnetic and acoustic cases, the canonical momentum density \mathbf{P} is determined by the quadratic form $\text{Im}[\mathbf{F}^* \cdot (\nabla)\mathbf{F}]$ entirely similar to the probability current in quantum mechanics, i.e., the local “expectation value” of the canonical quantum mechanical momentum operator $-i\nabla$ (29, 30). In turn, the spin angular momentum density \mathbf{S} is determined by the quadratic form $\text{Im}(\mathbf{F}^* \times \mathbf{F})$, which points into the direction normal to the polarization ellipse traced by the field $\mathbf{F}(\mathbf{r}, t)$ in a given point \mathbf{r} and is proportional to its ellipticity (16, 17, 39).

Notably, both electromagnetic and acoustic canonical momentum and spin densities in monochromatic fields are measurable via radiation forces and torques on small absorbing particles (17, 25, 27, 30). Note also that spatial integrals of the spin densities for localized circularly polarized paraxial electromagnetic waves and sound wave fields are in agreement with the quantum mechanical spin values of \hbar per photon (16, 17) and 0 per phonon (26, 28). Substituting the canonical momentum and spin densities into Eq. 1 and using the equations of motion for the wave fields (i.e., Maxwell and acoustic wave equations), one obtains the kinetic momentum density $\mathbf{\Pi}$. It is given by the well-known Poynting vector for electromagnetic waves and its acoustic analog for sound waves (31).

Importantly, the acoustic spin and canonical momentum densities can be immediately associated with the mechanical properties of microscopic particles of the medium. In general, such particles experience a combination of rotational and translational motion in the sound wave field. First, in the linear approximation, the microscopic periodic motion of the medium particles is generically elliptical and corresponds to the polarization of the vector velocity field \mathbf{v} . The oscillating velocity field $\mathbf{v}e^{-i\omega t}$ corresponds to the displacement field $\mathbf{a}e^{-i\omega t} = i\omega^{-1}\mathbf{v}e^{-i\omega t}$, which yields the time-averaged mechanical angular momentum density $(\rho/2) \text{Re}(\mathbf{a}^* \times \mathbf{v})$ (where ρ is the mass density of the medium) (23, 25, 28), precisely equivalent to the spin density \mathbf{S} in Table 1. Second, the medium particles in a sound wave field can experience the slow Stokes drift (36–38), a phenomenon known in hydrodynamics for surface water waves and related to the second-order difference between the Eulerian and Lagrangian velocities of the particles. [A somewhat related phenomenon of the transformation of an oscillatory motion to a linear drift is known as acoustic streaming (40), with numerous examples in acoustofluidics and surface acoustic waves (41, 42).] So far, the Stokes drift was described only for plane water surface waves with vertical inhomogeneity, while, here, we generalize this phenomenon to arbitrary inhomogeneous monochromatic fields. The momentum density associated with the generalized Stokes drift can be written as $(\rho/2) \text{Re}[(\mathbf{a}^* \cdot \nabla)\mathbf{v}]$ (see the Supplementary Materials), which, for sound waves with $\nabla \times \mathbf{v} = \mathbf{0}$, yields the canonical momentum density in Table 1. This expression is similar to the “pseudomomentum” of waves in fluids or gases introduced in 1978 by Andrews and McIntyre (43). Note, however, that the oscillatory and drift motions of particles in bulk sound waves are difficult to observe directly due to the very small displacements \mathbf{a} in typical sound wave fields.

Spin and momentum of gravity water waves

We now consider a wave system that is not typically associated with relativistic field theories and spin: water surface (gravity) waves. Deep-water gravity waves are characterized by the dispersion $\omega^2 = gk$, and all wave fields decay exponentially from the unperturbed water surface $z = 0$ deep into the water $z < 0$ as $\propto \exp(kz)$ (31). Thus, in contrast to the three-dimensional (3D) electromagnetism and acoustics, this system is quasi-2D. Since unperturbed water is translationally symmetric in the (x, y) plane and rotationally symmetric about the z axis, it is natural to expect a conserved 2D momentum and z -directed angular momentum of water waves. Therefore, we separate the 3D velocity \mathbf{v} of the water particles in the gravity wave field into the in-plane 2D vector $\mathbf{V} = (v_x, v_y)$ and the normal component $W = v_z$. We will focus on the 2D motion of surface water particles in the (x, y) plane ($z = 0$) but will also take into account all physical properties related to the vertical z motion. The 2D gradient

Table 1. The energy, momentum, and spin properties of electromagnetic, acoustic, and deep-water gravity monochromatic wave fields. Here, $c = 1/\sqrt{\epsilon\mu}$ is the speed of light, $c_s = 1/\sqrt{\beta\rho}$ is the speed of sound, ϵ and μ are the permittivity and permeability of the electromagnetic medium, whereas ρ and β are the mass density and compressibility of the acoustic medium or fluid.

	Electromagnetism	Acoustics	Water waves
Wave fields	Electric \mathbf{E} and magnetic \mathbf{H}	Velocity \mathbf{v} and pressure p	In-plane velocity \mathbf{V} and vertical velocity W
Energy density U	$\frac{1}{4}(\epsilon \mathbf{E} ^2 + \mu \mathbf{H} ^2)$	$\frac{1}{4}(\beta p ^2 + \rho \mathbf{v} ^2)$	$\frac{\rho}{4}(3 W ^2 + \mathbf{V} ^2)$
Kinetic momentum density $\mathbf{\Pi}$	$\frac{1}{2c^2}\text{Re}(\mathbf{E}^* \times \mathbf{H})$	$\frac{1}{2c_s^2}\text{Re}(p^* \mathbf{v})$	$\frac{\rho k}{\omega}\text{Im}(W^* \mathbf{V})$
Canonical momentum density \mathbf{P}	$\frac{1}{4\omega}\text{Im}[\epsilon \mathbf{E}^* \cdot (\nabla) \mathbf{E} + \mu \mathbf{H}^* \cdot (\nabla) \mathbf{H}]$	$\frac{\rho}{2\omega}\text{Im}[\mathbf{v}^* \cdot (\nabla) \mathbf{v}]$	$\frac{\rho}{2\omega}\text{Im}[\mathbf{V}^* \cdot (\nabla_2) \mathbf{V} + W^* \nabla_2 W]$
Spin AM density \mathbf{S}	$\frac{1}{4\omega}\text{Im}(\epsilon \mathbf{E}^* \times \mathbf{E} + \mu \mathbf{H}^* \times \mathbf{H})$	$\frac{\rho}{2\omega}\text{Im}(\mathbf{v}^* \times \mathbf{v})$	$\frac{\rho}{2\omega}\text{Im}(\mathbf{V}^* \times \mathbf{V})$

(momentum) operator is $\nabla_2 = (\partial_x, \partial_y)$, while the vector product (spin) operator “ \times ” acting in the plane can only produce a z -directed vertical spin.

Since the motion of water particles in the oscillating 2D velocity field $\mathbf{V}e^{-i\omega t}$ is entirely similar to the motion of medium particles in the oscillating sound wave field $\mathbf{v}e^{-i\omega t}$, the z -directed angular momentum density can be written akin to the acoustic spin density:

$$\mathbf{S} = \frac{\rho}{2\omega}\text{Im}(\mathbf{V}^* \times \mathbf{V}) \tag{2}$$

This provides the spin density for gravity waves associated with polarization of the vector field \mathbf{V} ; see Table 1. This spin appears in inhomogeneous (e.g., interference) water wave fields, because of the circular (or, generically, elliptical) motion of water particles in the (x, y) plane. Note that the spin Eq. 2 considered in our work is not the spin angular momentum considered by Longuet-Higgins in (44). The latter one is related to the elliptical motion of water particles in the propagation (z, x) plane (for x -propagating plane waves) and is directed along the horizontal y axis; our vertical spin Eq. 2 vanishes in a plane wave.

Next, the water particles experience the Stokes drift (36–38). So far, this phenomenon has been known for the circular motion of water particles in the plane orthogonal to the water surface, i.e., involving the vertical velocity component W . For inhomogeneous wave fields with a nonzero spin \mathbf{S} , the particles can also exhibit elliptical orbits in the projection onto the water surface plane. This produces the Stokes drift described by the in-plane velocity \mathbf{V} . Calculating the total Stokes drift in an arbitrary monochromatic gravity wave field, we obtain that its velocity \mathbf{u} is given by (see the Supplementary Materials)

$$\mathbf{u} = \frac{1}{2\omega}\text{Im}[\mathbf{V}^* \cdot (\nabla_2)\mathbf{V} + W^* \nabla_2 W], \quad \mathbf{P} = \rho\mathbf{u} \tag{3}$$

Here, by multiplying the Stokes drift velocity by the mass density, we obtained the canonical momentum density \mathbf{P} for gravity waves, analogous to the pseudomomentum by Andrews and McIntyre (43); see Table 1. The Stokes drift, i.e., the canonical momentum, produces mass transport in water waves (37), such as, e.g., the driftwood along the ocean coasts (45). For plane waves, $\mathbf{v} \propto \exp(i\mathbf{k} \cdot \mathbf{r})$, the generalized Stokes drift Eq. 3 is proportional to the wave vector:

$\mathbf{u} \propto \mathbf{k}$. This provides the natural similarity between the canonical momentum Eq. 3 and de Broglie momentum in quantum mechanics.

Now, substituting the above canonical momentum and spin densities into the Belinfante-Rosenfeld relation Eq. 1 and using the equations of motion for surface water wave fields, we obtain the kinetic momentum density $\mathbf{\Pi} = (\rho k/\omega)\text{Im}(W^* \mathbf{V})$ (see the Supplementary Materials and Table 1). Its form is equivalent to the conserved water wave momentum derived by Peskin (46). It should be noticed that the energy and momentum conservation laws for water waves are rather nontrivial, because they essentially involve z integrals of generic time-dependent fields (46). The energy and momentum densities are reduced to simple forms listed in Table 1 only for the case of monochromatic fields, when all fields decay as $\exp(kz)$, and the z integrals of quadratic forms are evaluated as $\int_{-\infty}^{\infty} dz = (2k)^{-1} \dots$

Moreover, unlike electromagnetic and acoustic waves, water surface waves cannot be described within a relativistic Lagrangian field theory. This can be seen from the fact that these waves are essentially dispersive, $\omega = \sqrt{gk}$, which breaks the Minkowski spacetime structure $\omega = ck$ underlying electromagnetic and acoustic field theories. It is not, by chance, that the electromagnetic field Lagrangian and conservation laws are described in any textbook in electromagnetism; the simplest energy conservation for sound waves can also be found in textbooks (31), although the acoustic field Lagrangian and other conservation laws are only present in more specialized literature; whereas water surface wave Lagrangian and conservation laws are absent in textbooks in hydrodynamics. [In addition, one of the most important works on water wave momentum (43) only shows the energy conservation law for bulk acoustic waves.] We summarize the main differences between electromagnetic, sound, and water surface waves in the Supplementary Materials. As remarked by Richard P. Feynman, water waves “are the worst possible example, because they are in no respects like sound and light; they have all the complications that waves can have”.

Probably the easiest ways to derive dynamical properties of water surface waves are (i) to use macroscopic wave equations of motion [as done by Peskin (46) in deriving the conserved kinetic momentum $\mathbf{\Pi}$] or (ii) to involve microscopic mechanical properties of water particles moving in wave fields (as done here in deriving canonical momentum \mathbf{P} and spin \mathbf{S}). Notably, both ways result in the kinetic and canonical densities exactly satisfying the Belinfante-Rosenfeld relation

Downloaded from https://www.science.org on January 28, 2022

Eq. 1 lying at the heart of relativistic field theory. This suggests that the Belinfante-Rosenfeld construction can have a deeper origin than a standard relativistic field theory. In general, one can expect that there is a nonrelativistic Lagrangian field theory for water surface waves with conserved energy, horizontal 2D momentum, and vertical angular momentum. However, such theory must involve a full description of the problem in the 3D bulk fluid (not only at the $z = 0$ surface), because the energy-momentum conservation for generic nonmonochromatic waves involves nontrivial z integrals of the fields (see the Supplementary Materials) (46). Constructing such Lagrangian formalism is an important problem for a separate study.

Importantly, the spin and momentum densities (Eqs. 2 and 3) are not abstract theoretical quantities but rather observable dynamical properties of surface gravity waves. We proceed with the direct experimental observation of these fundamental properties in structured water waves.

Examples and experimental measurements

We are now in a position to show explicit examples of surface gravity waves with nonzero spin and momentum. The first example is a simple interference of two plane waves with equal frequencies and orthogonal wave vectors $\mathbf{k}_1 \perp \mathbf{k}_2$. The spin and momentum in two-wave interference has been previously considered for optical and sound waves (25, 28, 47). Choosing the y axis to be directed along $\mathbf{k}_1 + \mathbf{k}_2$, the spin and canonical momentum densities, Eqs. 2 and 3, yield (see the Supplementary Materials)

$$\mathbf{S} \propto -\bar{\mathbf{z}} \sin \bar{x}, \quad \mathbf{P} \propto \bar{\mathbf{y}}(2 + \cos \bar{x}) \quad (4)$$

where $\bar{x} = \sqrt{2} kx$ and the overbar indicates the unit vectors of the corresponding axes. The distributions of these densities, together with the numerically calculated microscopic water particle trajectories, are shown in Fig. 1B. One can see that the canonical momentum density corresponds to the Stokes drift of the particles (which everywhere occurs in the y direction), whereas the spin density corresponds to the microscopic elliptical motion of particles (which has alternating x -dependent directions).

We have performed an experiment demonstrating the above motion of water particles and thereby the presence of canonical momentum and spin in the two-wave interference (Fig. 1). The experimental setup is shown in Fig. 1A (see the Supplementary Materials for details). Interfering gravity waves were generated in a wave tank with a size of $1.0 \times 0.6 \text{ m}^2$ and a depth of $h = 0.1 \text{ m}$ by two orthogonal paddles driven by two synchronized computer-controlled shakers. We worked with the wave frequencies $\omega/2\pi \in (3,9) \text{ Hz}$, which corresponds to the wavelengths $2\pi/k \in (0.03, 0.17) \text{ m}$ satisfying the deep-water condition $\tanh(kh) \approx 1$. Fluid motion at the water surface was visualized using buoyant tracer particles (polyamid, $50 \mu\text{m}$), illuminated by a light-emitting diode (LED) panel placed underneath the transparent wave tank. A video camera on top was used to capture the motion of the tracer particles.

In Fig. 1B, one can see that the experimentally measured trajectories are very similar to the numerically calculated ones. To show that these experimental observations are in quantitative agreement with the theoretical spin and momentum densities, we measure the spatial and frequency dependences of the drift velocities and rotational radii of the particles. First, the canonical momentum density should behave as $P_y \propto k/\omega \propto \omega$, because the gradient operator scales as $\propto k$. Obviously, the particle drift velocity u should obey the same frequency dependence. Second, the spin density is inversely proportional

to the frequency: $S_z \propto \omega^{-1}$. As we have discussed, the spin can be associated with the mechanical angular momentum of water particles. At the points of maximum absolute value of the spin, $\bar{x} = \pm \pi/2$, the water particles follow near circular orbits of radius a (see Fig. 1B), and their angular momentum is $\propto a^2 \omega$. Therefore, this radius should depend on the frequency as $a \propto \omega^{-1}$. Figure 2 shows the experimentally measured dependences $u(\omega)$ and $a(\omega)$ for water particles. These dependences are in excellent agreement with the above theoretical predictions and the x dependence $\propto (2 + \cos \bar{x})$ of the canonical momentum Eq. 4. The only discrepancy is that the drift velocity is offset by a constant value such that $u(0) \neq 0$. This is due to the presence of small return flows in the finite-size wave tank (see the Supplementary Materials).

As another example, we consider an interference of two orthogonal standing water waves with equal amplitudes and frequencies, which is equivalent to four propagating waves. In this case, the spin density Eq. 2 forms a periodic chessboard-like structure, whereas the canonical momentum density Eq. 3 forms vortex-like flows around the maxima and minima of the spin density (see the Supplementary Materials and Fig. 3) (48):

$$\mathbf{S} \propto \bar{\mathbf{z}} \sin \varphi \cos \bar{x} \cos \bar{y}, \quad \mathbf{P} \propto \sin \varphi (\bar{\mathbf{y}} \sin \bar{x} \cos \bar{y} - \bar{\mathbf{x}} \cos \bar{x} \sin \bar{y}) \quad (5)$$

Here, $\bar{x} = kx$, $\bar{y} = ky$, and φ is the phase between the two orthogonal standing waves. Figure 3 shows the numerically calculated and experimentally measured trajectories of microscopic particles in the interference of two orthogonal standing waves with $\varphi = \pi/2$ (the spinless case $\varphi = 0$ is shown in the Supplementary Materials). One can see that particles follow large wavelength-scale vortex-like orbits due to the Stokes drift associated with the canonical momentum \mathbf{P} . Simultaneously, the particles experience microscopic elliptical motion around their current positions, which produces the local angular momentum associated with the spin \mathbf{S} . We emphasize that the two orbital motions here have different scales and qualitatively different nature. The radius of the microscopic spin-related circular motion is proportional to the amplitude of the wave and can be made as small as needed, while the radius of the macroscopic vortex-like motion is fixed by the wavelength.

Note that the experimentally measured fluid particle trajectories shown in Fig. 1B, particularly their unidirectional Stokes drift, were only observed transiently during the first stage of the flow development. As the flow evolves, the trochoidal Stokes orbits bend, as illustrated in Fig. 4: Opposite spins slowly drift in opposite transverse directions. This behavior can be interpreted as a water wave analog of the spin Hall effect, a universal manifestation of spin-orbit interactions known in condensed matter physics (49), optics (20), and even having implications in hydrodynamics (50). This is still a transient behavior in the propagating waves configuration, and the conservation of mass in the top fluid layer leads to the development of return currents that decrease the mean drift velocity in the regions $\bar{x} \in \pm (\pi, 2\pi)$. In addition, in a finite-size basin, reflected waves also distort the original propagating wave field, thereby contributing to the further distortion of the surface flow. Thus, truly stationary flow patterns only form in the crossed standing wave configuration, as in Fig. 3, where bending of the trajectories leads to the formation of closed loops and return flows do not arise.

DISCUSSION

To conclude, we have revealed the fundamental spin and momentum properties in water surface (gravity) waves. These quantities are

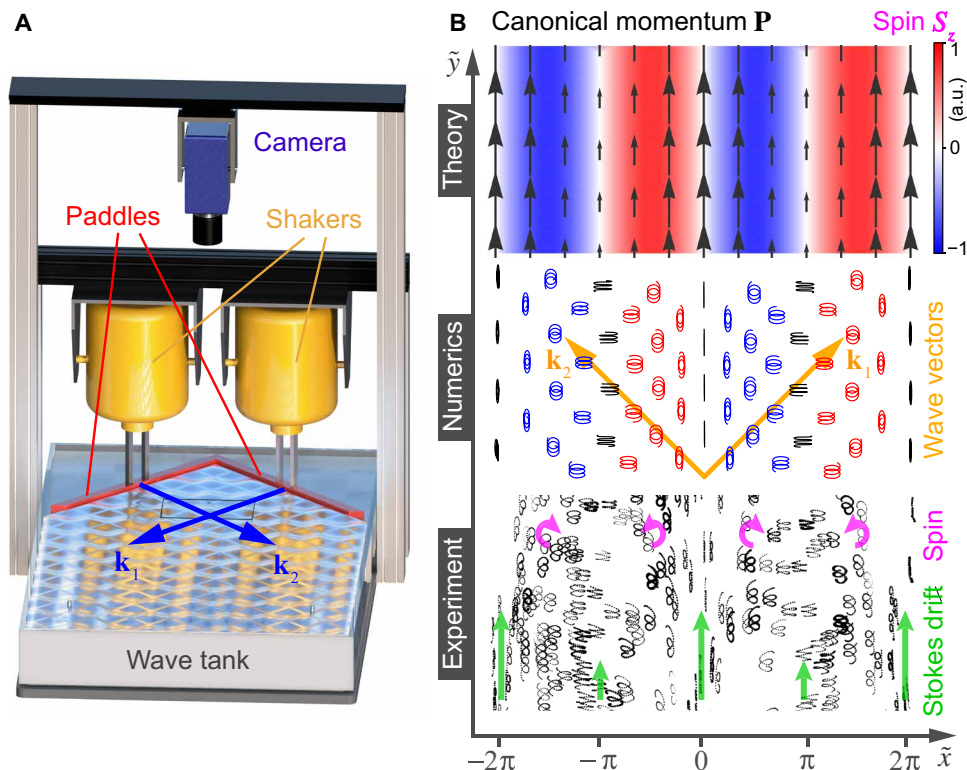


Fig. 1. The canonical momentum and spin densities in the interference of two gravity waves. (A) Schematic of the experimental setup for the observation of the particle motion in interfering water surface waves. (B) Spin and momentum properties of two interfering gravity waves with equal frequencies, amplitudes, and orthogonal wave vectors k_1 and k_2 . The theoretical plot shows the distributions of the canonical momentum density P and spin density S (Table 1). Numerical and experimental plots depict trajectories of microscopic particles for three wave periods $6\pi/\omega$. The Stokes drift of the particles and their elliptical motion correspond to the canonical momentum and spin, respectively. Parameters are $\bar{x} = \sqrt{2}k_x x$, $\bar{y} = \sqrt{2}k_y y$, and $\omega/2\pi = 6$ Hz. a.u., arbitrary units.

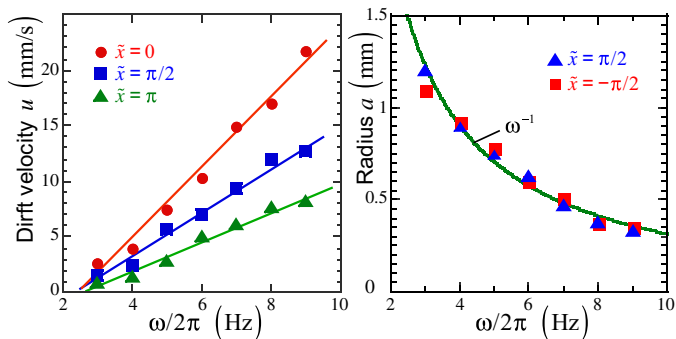


Fig. 2. Frequency dependencies of the Stokes drift and the microscopic orbits in interfering gravity waves from Fig. 1. The experimentally measured Stokes drift velocity grows linearly with the wave frequency and depends on the position $\bar{x} = \sqrt{2}k_x x$. The radii of the circular motion of water particles at the maxima of the spin density are inversely proportional to the wave frequency. These dependences are in agreement with theoretical predictions based on the canonical momentum and spin densities Eqs. 2 to 5.

precisely described by the relativistic field theory construction by Belinfante-Rosenfeld (4–6), which underpins the spin and momentum of quantum and classical particles and fields. We have shown that the canonical momentum density in acoustic and water waves can be directly associated with the mass transfer due to the generalized Stokes drift, while the spin density originates from the mechanical

angular momentum of the medium particles following microscopic elliptical trajectories. We have provided the direct observation of these drift and rotational dynamics of water particles in inhomogeneous gravity wave fields. This can be regarded as the first direct observation of the microscopic origin of the canonical spin and momentum in structured wave fields.

The appearance of a relativistic field theory construction in the properties of water surface waves is rather unexpected. Such waves can be associated with relativistic field theory neither physically nor mathematically. Their dispersion is inconsistent with the Minkowski-like space-time symmetries, whereas a simple (2 + 1)D form of the equations of motion does not have even the basic energy conservation law (see the Supplementary Materials). Nonetheless, the presence of the (2 + 1)D space-time symmetries and microscopic mechanical description of the motion of the medium molecules in water wave fields allows one to obtain meaningful (x, y) momentum and z-directed angular momentum of water waves. These quantities involve z-directed spin and are exactly described by the Belinfante-Rosenfeld relation. This hints that the Belinfante-Rosenfeld relation has a more fundamental origin than relativistic field theory.

Our results can have a multifold interdisciplinary impact. They shed light onto the nature of spin and momentum in various wave fields and illuminate the universality of field theory relations, which, so far, have been considered as abstract theoretical entities underlying observable physical phenomena on a higher level. Our findings also unveil the nontrivial nature of water wave and acoustic momentum,

Downloaded from https://www.science.org on January 28, 2022

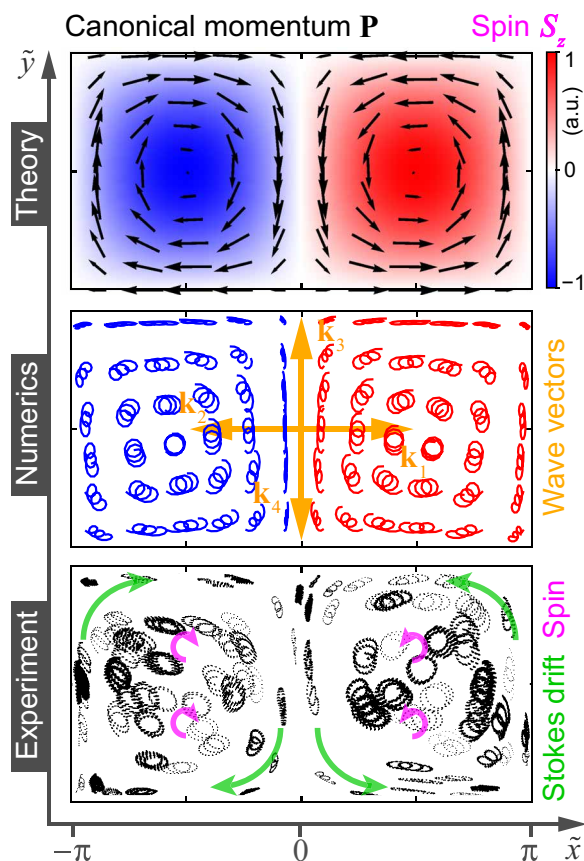


Fig. 3. Canonical momentum and spin densities in the interference of two standing gravity waves. Same as in Fig. 1 but for two interfering orthogonal standing waves with equal frequencies and amplitudes (i.e., equivalently, four propagating plane waves with the wave vectors $\mathbf{k}_{1,2,3,4}$). Parameters are $\tilde{x} = kx$, $\tilde{y} = ky$, and $\omega/2\pi = 5.3$ Hz.

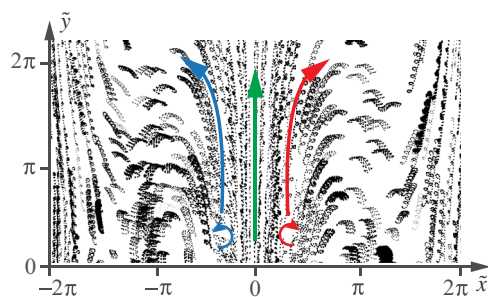


Fig. 4. Water wave analog of the spin Hall effect. Experimentally measured trajectories of water particles in two interfering waves, same as in Fig. 1B, but for a longer period of time (about 10 wave periods). The forward propagation of spinning particles due to the Stokes drift is accompanied by the transverse splitting of oppositely spinning particles.

which caused longstanding discussions (43, 46, 51, 52). The presence of nonzero spin density explains the existence of two (canonical and kinetic) momenta and the direct observability of at least one of these. Our experiments provide direct measurements of the local mass transport in structured water surface waves. Notably, using the dynamical spin and momentum concepts, one can produce structured

water wave fields for desired manipulation of particles, including transport and rotation, akin to optical manipulations (16, 17, 27, 53).

MATERIALS AND METHODS

A schematic of the experiment is shown in Fig. 1A (see also the Supplementary Materials). Surface gravity waves are generated in a wave tank of size 1.0 m by 0.6 m. The water depth is kept at $h = 0.1$ m to ensure the deep-water approximation for the surface waves, i.e., $\tanh(kh) \approx 1$, where the wave numbers are in the range of $k = (36 \text{ to } 233) \text{ m}^{-1}$ for the wave frequencies of $\omega/2\pi = (3 \text{ to } 9)$ Hz. Sinusoidal waves are produced by two vertically oscillating paddles oriented at 90° with respect to each other, as shown in Fig. 1A. The computer-controlled electrodynamic shakers (TIRA TV51140) drive the synchronized motion of two wave paddles. The paddle accelerations are measured using two accelerometers (Brüel & Kjær 4507), which provide feedback to the motion controllers (Vibration Research, VR9500). The phase delay φ between the paddles is adjustable in the range of $(-\pi, \pi)$ with an accuracy of ± 0.002 using a two-channel arbitrary waveform generator (HP 33120 A).

In the propagating wave configuration, a shallow beach (inclined perspex plate) and an egg shell absorber at the end of the wave tank are used to minimize wave reflections. In the standing wave configuration, two wave-reflecting boundaries together with the wave paddles form a resonant square cavity of size L , which accommodates an integer number N of wavelengths, $L = 2\pi N/k = 2\pi N g/\omega^2$.

The fluid motion at the water surface is visualized using buoyant tracer particles (polyamid, $50 \mu\text{m}$), illuminated by an LED panel placed underneath the transparent wave tank. A video camera (2560×2160 pixel, 100 fps; Andor Zyla X5.5) with a Nikon f1.4/50 mm lens is used to capture the motion of the tracer particles. The videos are processed and analyzed using the ImageJ software package.

The surface flows in a finite-size container can be distorted by return flows. For this reason, the tracer particle trajectories are analyzed for the first 10 wave periods, $t \in (0, 20\pi/\omega)$, i.e., shortly after the onset of the wave field, to avoid the flow distortion due to the gradual buildup of the return surface flows. Special care is also taken to avoid flows and secondary waves originating from menisci appearing along the contact lines between water, the container walls, and the wave paddles. This is achieved by machining grooves on the paddles and the container boundaries at the level of the unperturbed water surface.

We compare the experimentally measured trajectories with the numerically computed trajectories shown in the middle Fig. 1B. The numerical trajectories are computed by integrating the time-dependent velocity field, $\mathbf{V}(\mathbf{r}, t) = \text{Re}[\mathbf{V}(\mathbf{r})e^{-i\omega t}]$, using the fourth-order Runge-Kutta method.

SUPPLEMENTARY MATERIALS

Supplementary material for this article is available at <https://science.org/doi/10.1126/sciadv.abm1295>

REFERENCES AND NOTES

- G. E. Uhlenbeck, S. Goudsmit, Spinning electrons and the structure of spectra. *Nature* **117**, 264–265 (1926).
- Spin, *Nature Milestones* S5–S20 (2008); <https://www.nature.com/collections/idgejiafca/#:~:text=The%20Milestones%20are%20a%20series,reviews%20from%20Nature%20Publishing%20Group>
- V. B. Berestetskii, E. M. Lifshitz, L. P. Pitaevskii, *Quantum Electrodynamics* (1982).
- F. J. Belinfante, On the current and the density of the electric charge, the energy, the linear momentum and the angular momentum of arbitrary fields. *Physica* **7**, 449–474 (1940).

5. L. Rosenfeld, On the energy-momentum tensor. *Memoirs Acad. Roy. de Belgique* **18**, 1–30 (1940).
6. D. E. Soper, *Classical Field Theory* (Wiley, 1976).
7. H. C. Ohanian, What is spin? *Am. J. Phys.* **54**, 500–505 (1986).
8. S. A. Wolf, D. D. Awschalom, R. A. Buhrman, J. M. Daughton, S. von Molnar, M. L. Roukes, A. Y. Chtchelkanova, D. M. Treger, Spintronics: A spin-based electronics vision for the future. *Science* **294**, 1488–1495 (2001).
9. I. Zutic, J. Fabian, S. Das Sarma, Spintronics: Fundamentals and applications. *Rev. Mod. Phys.* **76**, 323–410 (2004).
10. I. Buluta, S. Ashhab, F. Nori, Natural and artificial atoms for quantum computation. *Rep. Prog. Phys.* **74**, 104401 (2011).
11. J. J. Pla, K. Y. Tan, J. P. Dehollain, W. H. Lim, J. J. L. Morton, D. N. Jamieson, A. S. Dzurak, A. Morello, A single-atom electron spin qubit in silicon. *Nature* **489**, 541–545 (2012).
12. L. M. K. Vandersypen, H. Bluhm, J. S. Clarke, A. S. Dzurak, R. Ishihara, A. Morello, D. J. Reilly, L. R. Schreiber, M. Veldhorst, Interfacing spin qubits in quantum dots and donors—hot, dense, and coherent. *npj Quantum Inf.* **3**, 34 (2017).
13. J. H. Poynting, The wave-motion of a revolving shaft, and a suggestion as to the angular momentum in a beam of circularly-polarized light. *Proc. R. Soc. Lond. A* **82**, 560–567 (1909).
14. R. A. Beth, Mechanical detection and measurement of the angular momentum of light. *Phys. Rev.* **50**, 115–125 (1936).
15. N. B. Simpson, K. Dholakia, L. Allen, M. J. Padgett, Mechanical equivalence of spin and orbital angular momentum of light: An optical spanner. *Opt. Lett.* **22**, 52–54 (1997).
16. *The Angular Momentum of Light*, D. L. Andrews, M. Babiker, Eds. (Cambridge Univ. Press, 2013).
17. K. Y. Bliokh, F. Nori, Transverse and longitudinal angular momenta of light. *Phys. Rep.* **592**, 1–38 (2015).
18. R. P. Cameron, S. M. Barnett, A. M. Yao, Optical helicity, optical spin and related quantities in electromagnetic theory. *New J. Phys.* **14**, 053050 (2012).
19. K. Y. Bliokh, A. Y. Bekshaev, F. Nori, Dual electromagnetism: Helicity, spin, momentum and angular momentum. *New J. Phys.* **15**, 033026 (2013).
20. K. Y. Bliokh, F. J. Rodríguez-Fortuño, F. Nori, A. V. Zayats, Spin-orbit interactions of light. *Nat. Photonics* **9**, 796–808 (2015).
21. A. Aiello, P. Banzer, M. Neugebauer, G. Leuchs, From transverse angular momentum to photonic wheels. *Nat. Photonics* **9**, 789–795 (2015).
22. P. Lodahl, S. Mahmoodian, S. Stobbe, A. Rauschenbeutel, P. Schneeweiss, J. Volz, H. Pichler, P. Zoller, Chiral quantum optics. *Nature* **541**, 473–480 (2017).
23. W. L. Jones, Asymmetric wave-stress tensors and wave spin. *J. Fluid Mech.* **58**, 737–747 (1973).
24. Y. Long, J. Ren, H. Chen, Intrinsic spin of elastic waves. *Proc. Natl. Acad. Sci. U.S.A.* **115**, 9951–9955 (2018).
25. C. Shi, R. Zhao, Y. Long, S. Yang, Y. Wang, H. Chen, J. Ren, X. Zhang, Observation of acoustic spin. *Natl. Sci. Rev.* **6**, 707–712 (2019).
26. K. Y. Bliokh, F. Nori, Spin and orbital angular momenta of acoustic beams. *Phys. Rev. B* **99**, 174310 (2019).
27. I. D. Toftul, K. Y. Bliokh, M. I. Petrov, F. Nori, Acoustic radiation force and torque on small particles as measures of the canonical momentum and spin densities. *Phys. Rev. Lett.* **123**, 183901 (2019).
28. L. Burns, K. Y. Bliokh, F. Nori, J. Dressel, Acoustic versus electromagnetic field theory: Scalar, vector, spinor representations and the emergence of acoustic spin. *New J. Phys.* **22**, 053050 (2020).
29. M. V. Berry, Optical currents. *J. Opt.* **11**, 094001 (2009).
30. K. Y. Bliokh, A. Y. Bekshaev, F. Nori, Extraordinary momentum and spin in evanescent waves. *Nat. Commun.* **5**, 3300 (2014).
31. L. D. Landau, E. M. Lifshitz, *Fluid Mechanics* (Butterworth-Heinemann, 1987).
32. R. L. Seliger, G. B. Whitham, Variational principles in continuum mechanics. *Proc. R. Soc. Lond. A* **305**, 1–25 (1968).
33. L. J. F. Broer, On the Hamiltonian theory of surface waves. *Appl. Sci. Res.* **30**, 430–446 (1974).
34. T. Brooke Benjamin, P. J. Olver, Hamiltonian structure, symmetries and conservation laws for water waves. *J. Fluid Mech.* **125**, 137–185 (1982).
35. T. G. Shepherd, Symmetries, conservation laws, and Hamiltonian structure in geophysical fluid dynamics. *Adv. Geophys.* **32**, 287–338 (1990).
36. G. G. Stokes, On the theory of oscillatory waves. *Trans. Cambridge Philos. Soc.* **8**, 441–455 (1847). Reprinted in G.G. Stokes, *Mathematical and Physical Papers*, vol. 1 (Cambridge Univ. Press, 1880).
37. M. S. Longuet-Higgins, Mass transport in water waves. *Philos. Trans. R. Soc. A* **245**, 535–581 (1953).
38. T. S. van den Bremer, Ø. Breivik, Stokes drift. *Philos. Trans. R. Soc. A* **376**, 20170104 (2017).
39. M. V. Berry, M. R. Dennis, Polarization singularities in isotropic random vector waves. *Proc. R. Soc. Lond. A* **457**, 141–155 (2001).
40. N. Riley, Acoustic streaming. *Theor. Comput. Fluid Dyn.* **10**, 349–356 (1998).
41. J. Friend, L. Y. Yeo, Microscale acoustofluidics: Microfluidics driven via acoustics and ultrasonics. *Rev. Mod. Phys.* **83**, 647–704 (2011).
42. W. Connacher, N. Zhang, A. Huang, J. Mei, S. Zhang, T. Gopesh, J. Friend, Micro/nano acoustofluidics: Materials, phenomena, design, devices, and applications. *Lab Chip* **18**, 1952–1996 (2018).
43. D. G. Andrews, M. E. McIntyre, On wave-action and its relatives. *J. Fluid Mech.* **89**, 647–664 (1978).
44. M. S. Longuet-Higgins, Spin and angular momentum in gravity waves. *J. Fluid Mech.* **97**, 1–25 (1980).
45. M. Kubota, A mechanism for the accumulation of floating marine debris north of Hawaii. *J. Phys. Oceanogr.* **24**, 1059–1064 (1994).
46. C. S. Peskin, Wave momentum (The Silver Dialogues, New York Univ., 2010); www.math.nyu.edu/faculty/peskin/papers/wave_momentum.pdf.
47. A. Y. Bekshaev, K. Y. Bliokh, F. Nori, Transverse spin and momentum in two-wave interference. *Phys. Rev. X* **5**, 011039 (2015).
48. N. Francois, H. Xia, H. Punzmann, P. W. Fontana, M. Shats, Wave-based liquid-interface metamaterials. *Nat. Commun.* **8**, 14325 (2017).
49. J. Sinova, S. O. Valenzuela, J. Wunderlich, C. H. Back, T. Jungwirth, Spin Hall effects. *Rev. Mod. Phys.* **87**, 1213–1260 (2015).
50. R. Takahashi, M. Matsuo, M. Ono, K. Harii, H. Chudo, S. Okayasu, J. Ieda, S. Takahashi, S. Maekawa, E. Saitoh, Spin hydrodynamic generation. *Nat. Phys.* **12**, 52–56 (2016).
51. M. E. McIntyre, On the “wave momentum” myth. *J. Fluid Mech.* **106**, 331–347 (1981).
52. M. Stone, Phonons and forces: Momentum versus pseudomomentum in moving fluids, in *Artificial Black Holes*, M. Novello, M. Visser, G. Volovik, Eds. (World Scientific, 2002).
53. D. G. Grier, A revolution in optical manipulation. *Nature* **424**, 810–816 (2003).
54. J. Lighthill, *Waves in Fluids* (Cambridge Univ. Press, 2001).
55. K. Y. Bliokh, D. Smirnova, F. Nori, Quantum spin Hall effect of light. *Science* **348**, 1448–1451 (2015).
56. K. Y. Bliokh, F. Nori, Transverse spin and surface waves in acoustic metamaterials. *Phys. Rev. B* **99**, 020310 (R) (2019).
57. M. Visser, Emergent rainbow spacetimes: Two pedagogical examples; arXiv:0712.0810 (2007).

Acknowledgments: We acknowledge fruitful discussions with L. Burns and J. Dressel.

Funding: This work was partially supported by the Australian Research Council (ARC) via the Discovery Grants DP160100863 and DP190100406, Nippon Telegraph and Telephone Corporation (NTT) Research, the Japan Science and Technology Agency (JST) via the Moonshot R&D grant no. JP-MJMS2061 and the Centers of Research Excellence in Science and Technology (CREST) grant no. JPMJCR1676, the Japan Society for the Promotion of Science (JSPS) via the Grants-in-Aid for Scientific Research (KAKENHI) grant no. JP20H00134 and the JSPS-RFBR grant no. JPJSBP120194828, the Army Research Office (ARO) via grant no. W911NF-18-1-0358, the Asian Office of Aerospace Research and Development (AOARD) via grant no. FA2386-20-1-4069, and the Foundational Questions Institute Fund (FQXi) via grant no. FQXi-IAF19-06. **Author contributions:** K.Y.B. provided theoretical background for this research, made theoretical calculations, and prepared the manuscript with input from M.S., H.P., and F.N. H.P. and M.S. designed the experimental setup, performed experiments, and analyzed the data. H.X. performed numerical modeling of the fluid particle trajectories. All authors discussed and edited the manuscript. **Competing interests:** The authors declare that they have no competing interests. **Data and materials availability:** All data needed to evaluate the conclusions in the paper are present in the paper and/or the Supplementary Materials.

Submitted 27 August 2021

Accepted 29 November 2021

Published 21 January 2022

10.1126/sciadv.abm1295

Field theory spin and momentum in water waves

Konstantin Y. BliokhHorst PunzmannHua XiaFranco NoriMichael Shats

Sci. Adv., 8 (3), eabm1295. • DOI: 10.1126/sciadv.abm1295

View the article online

<https://www.science.org/doi/10.1126/sciadv.abm1295>

Permissions

<https://www.science.org/help/reprints-and-permissions>

Use of think article is subject to the [Terms of service](#)